Understanding the varied response of the extratropical storm tracks to climate change

Paul A. O'Gorman[1]

Massachusetts Institute of Technology, Cambridge, MA 02139

Transient eddies in the extratropical storm tracks are a primary mechanism for the transport of momentum, energy, and water in the atmosphere, and as such are a major component of the climate system. Changes in the extratropical storm tracks under global warming would impact these transports, the ocean circulation and carbon cycle, and society through changing weather patterns. I show that the southern storm track intensifies in the multimodel mean of simulations of 21st century climate change, and that the seasonal cycle of storm-track intensity increases in amplitude in both hemispheres. I use observations of the present-day seasonal cycle to confirm the relationship between storm-track intensity and the mean available potential energy of the atmosphere, and show how this quantitative relationship can be used to account for much of the varied response in storm-track intensity to global warming, including substantially different responses in simulations with different climate models. The results suggest that storm-track intensity is not related in a simple way to global-mean surface temperature, so that, for example, a stronger southern storm track in response to present-day global warming does not imply it was also stronger in hothouse climates of the past.

It is a basic question in climate science as to whether the transient eddies that make up the extratropical storm tracks were stronger or weaker in warmer or colder climates (1–8), or if indeed there is an "optimally stormy" climate state (4, 8). Changes in eddy intensity under global warming would impact the ocean circulation, carbon cycle (9), and society through changing weather patterns (10, 11). There is a poleward shift of the storm tracks in some simulations of global-warming scenarios (2, 5, 12), and possibly in recent decades in observations (13, 14). But the simulated response of the storm tracks to global warming is not purely a shift poleward; it also involves comparable changes in overall intensity. The changes in intensity are less widely appreciated, in part, because they are strongly dependent on the season and hemisphere in question, whereas the shift (when present) is generally poleward with warming.

To examine this varied response in intensity, I have analyzed the changes in kinetic energy of the extratropical storm tracks in climate model simulations of a global-warming scenario and how they relate to changes in the mean state of the atmosphere. The simulations analyzed are drawn from the World Climate Research Programme's Coupled Model Intercomparison Project phase 3 archive (*Methods*). The results are presented in terms of the changes in the transient eddy kinetic energy (EKE) averaged over two 20-y periods at the ends of the 20th and 21st centuries, under a moderate emissions scenario for greenhouse gases [Special Report on Emissions Scenarios (SRES) A1B].

Results

First consider the distribution of EKE in the multimodel mean and its changes in boreal summer [June-July-August (JJA)]. The climatological storm tracks are localized in the extratropics of both hemispheres, and are stronger in the winter hemisphere (Fig. 1*A*). The changes in EKE indicate a strengthening of the eddies over the Southern Ocean, and a general weakening over most of the northern hemisphere (Fig. 1*B*). The annual-mean response also features a strengthening in the southern hemisphere
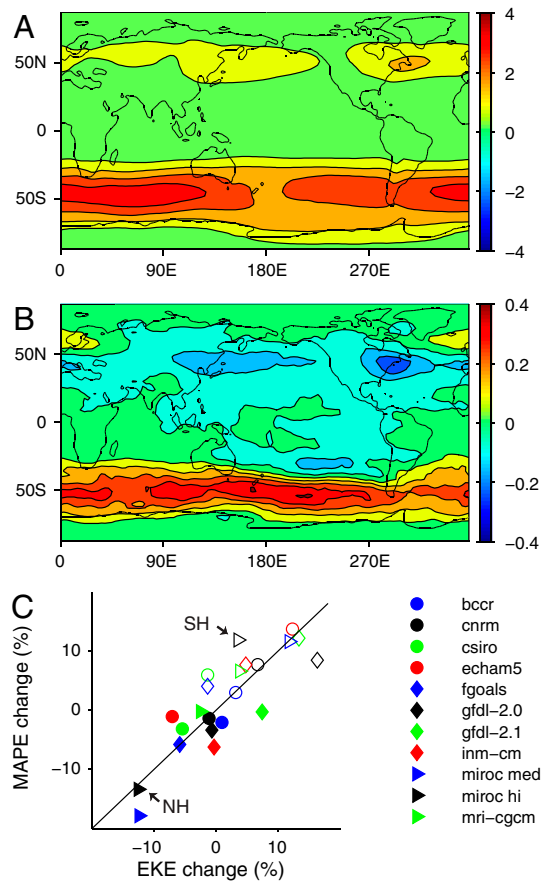
Fig. 1. Storm-track intensity in JJA in climate model simulations: (*A*) Transient EKE (10^5 J m^{-2}) averaged from 1981 to 2000 and in the multimodel mean (with slightly different time periods for some models; *Methods*). (*B*) Changes in multimodel mean EKE under global warming, calculated as the difference between time averages over 1981–2000 and 2081–2100. (*C*) Fractional changes in EKE and nonconvective MAPE under global warming for each model. Values are given for the northern hemisphere (solid symbols) and southern hemisphere (open symbols), but excluding the deep tropics (below 20° latitude in each hemisphere). The solid line indicates the one-to-one relationship corresponding to linear scaling of EKE and MAPE.

(Fig. S1), but there is a pronounced poleward shift in both hemispheres in December-January-February (DJF), with little change in intensity in the multimodel mean (Fig. 2*C* and Fig. S2). The changes in EKE in both hemispheres tend to amplify the seasonal

cycle in storminess as the climate warms, in combination with a general strengthening in the southern hemisphere (Fig. 2C). The amplification of the seasonal cycle in EKE is robust across the different climate models; the absolute value of the difference in EKE between DJF and JJA increases in 10 out of 11 models (and by 19% in the multimodel mean) in the southern hemisphere, and in 8 out of 11 models (and by 6% in the multimodel mean) in the northern hemisphere. But the changes in EKE are not generally consistent between the different climate model simulations. For example, although the changes in EKE in JJA in the southern hemisphere are almost all positive, they range from −1% to +16% (Fig. 1C). Normalization by the change in global-mean surface temperature does not reduce this scatter.

Mean Available Potential Energy. What determines the asymmetry of the changes in intensity of the storm tracks in the two hemispheres, their seasonal dependence, and the varying responses in different climate models? A warmer and moister atmosphere under global warming has greater internal, latent, and gravitational potential energy. But only a small part of the internal, latent, and gravitational potential energy associated with the mean state of the atmosphere is available for conversion to kinetic energy (15, 16). This part of the energy of the mean state is termed "mean available potential energy" (MAPE), which increases with increasing horizontal temperature gradients and decreasing static stability, and is always greater when the latent heat release associated with phase changes of water is taken into account (15). MAPE quantitatively combines in a consistent way the many factors that have been proposed to affect storm-track
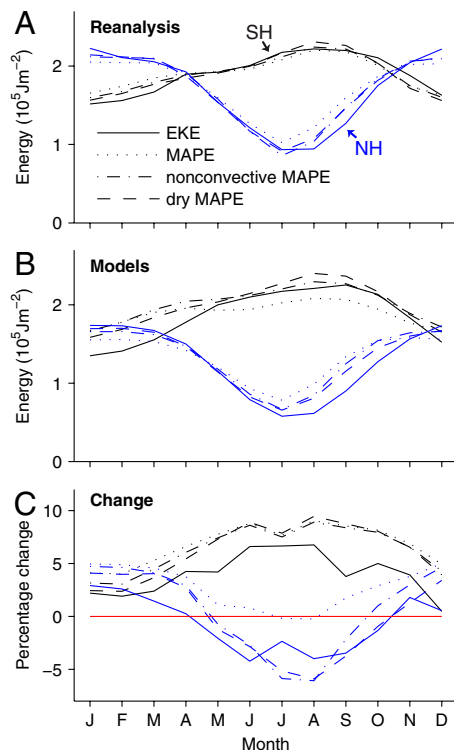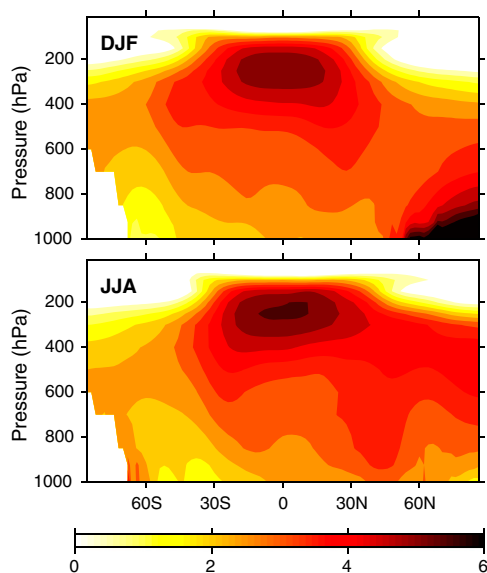

Fig. 2. Seasonal variations of EKE and three types of (rescaled) MAPE: (A) The NCEP-DOE reanalysis (1981–2000). (B) The multimodel mean (1981–2000). (C) The multimodel mean of the fractional changes in EKE and MAPE under global warming. The full MAPE (dotted), nonconvective MAPE (dash-dotted), and dry MAPE (dashed) are shown for the southern hemisphere (black) and northern hemisphere (blue). The MAPE curves for each hemisphere in A and B have been rescaled by multiplicative constants determined by a least-squares fit (linear with zero intercept) to the corresponding EKE curves. Numerical values for each type of MAPE are detailed in Table S1.

intensity, such as horizontal temperature gradients and latent heat release.

A linear scaling between EKE and MAPE (EKE $\sim c$ MAPE, where c is a constant) is expected based on theories of baroclinic turbulence in two-layer quasigeostrophic models if the supercriticality is assumed to remain roughly constant (17). The applicability of this scaling to more fully dynamical atmospheres is difficult to show from theory, but it has been found to hold empirically over a wide range of climates in simulations with dry and moist idealized general circulation models (8, 18). Even nonmonotonic changes in storm-track intensity as a function of global-mean surface temperature were captured by the MAPE scaling, and were found to result from competing effects such as different changes in temperature gradients at different levels in the atmosphere (8). Storm-track intensity feeds back on the mean temperature structure of the atmosphere by influencing the magnitude of moist static energy fluxes, so that care must be taken in arguing the causality of changes in MAPE and EKE. But the changes in poleward energy fluxes are dominated by changes in latent heat flux due to increasing specific humidities rather than changes in circulation strength (19), so that the scaling of EKE and MAPE remains a promising means to reason about the changes in intensity of the extratropical storm tracks under climate change.

I first confirm that the linear scaling between MAPE and EKE holds in observations of the seasonal cycle in the present climate (Fig. 2A). The observational estimates are based on the National Centers for Environmental Prediction–Department of Energy (NCEP-DOE) reanalysis (20), and suggest a tight and linear relationship between EKE and MAPE, with maximal EKE and MAPE in winter in each hemisphere. A similar scaling relationship holds in the climate model simulations, albeit slightly less accurately (Fig. 2B). The accuracy of the scaling over the seasonal cycle is roughly as good whether the effects of water vapor are included (MAPE) or not included (dry MAPE), even though the effect of latent heat release is to increase MAPE (Tables S1 and S2). The accuracy of the scaling is also similar in the two hemispheres, despite the more complicated energy cycle in the northern hemisphere because of greater stationary wave activity.

The scaling with MAPE also captures the main features of the changes in EKE under climate change, including the order of magnitude of the response, the increases throughout the year in the southern hemisphere, and the tendency to amplify the seasonal cycle in EKE in both hemispheres (Fig. 2C). There is, however, some dependence on whether water vapor is included in the calculation (MAPE versus dry MAPE), and this dependence is found to be related to small-scale convective overturning circulations*. To quantify the energy available to the large-scale flow, I introduce a "nonconvective" MAPE which does not allow the reordering of the pressure of air parcels originating in a given column of air, although it does allow for latent heat release (Methods). Nonconvective MAPE is intermediate in value between dry MAPE and MAPE (Tables S1 and S2), but scales more like dry MAPE under climate change (Fig. 2C). This scaling behavior suggests a diminished role for the effect of increasing amounts of atmospheric water vapor on large-scale extratropical eddies.

Relation to the Pattern of Temperature Changes. Having confirmed the scaling of EKE and MAPE, I now analyze the reasons for the wide range of changes in MAPE depending on hemisphere, season, and climate model. The calculation of MAPE only involves

---

*Inspection of the adiabatic rearrangements of mass involved in the calculation of MAPE reveals that the differences in the changes in MAPE and dry MAPE are primarily related to the release of convective instability as high entropy air rises (Fig. S3). Release of convective instability involves overturning circulations on short horizontal length scales, irreversible mixing, and local dissipation of kinetic energy (21). But the kinetic energy associated with convective overturning does not necessarily contribute to the large-scale kinetic energy of eddies; it may be dissipated locally before any upscale energy transfer occurs.

time-averaged and zonally averaged temperature and humidity fields. Increasing atmospheric water vapor amounts under global warming will tend to increase MAPE, but, as seen earlier, the dry MAPE and nonconvective MAPE scale similarly, and therefore water vapor may not play a major role directly. Water vapor does however play a role in helping to determine the changes in the thermal structure of the atmosphere (8, 22). There is a pronounced peak in warming in the tropical troposphere, leading to an increase in the southern hemispheric meridional temperature gradient and MAPE throughout the year (Fig. 3). But the northern high-latitude warming patterns depend strongly on season, with a peak in warming near the surface in winter, and more warming higher in the atmosphere in summer. This pattern of warming in the Arctic is partly related to ice-albedo feedback (23), but also involves interactions between the atmosphere, melting sea ice, and the ocean mixed layer. Consideration of only the surface meridional temperature gradient would suggest a weakening of northern hemispheric eddies in DJF and little change in JJA, the opposite of the seasonality of changes found in the simulations (Fig. 2C). In terms of MAPE, the strong decrease in near-surface temperature gradient in DJF is counteracted by increased meridional temperature gradients in the upper troposphere and decreases in static stability, to give a slightly positive change in energy. In the JJA season, the decrease in MAPE in the northern hemisphere is partly related to increased static stability. The link between EKE and MAPE allows us to relate the amplification in the seasonal cycle of storm-track intensity to seasonal changes in the thermal structure of the troposphere; the underlying reason for the amplification of the seasonal cycle in MAPE deserves further investigation, given the robustness of this response across the models.

The changes in both hemispheres make clear that consideration of only the surface meridional temperature gradient is inadequate for understanding changes in the intensity of the storm tracks (it would suggest little change in the southern hemisphere and the opposite seasonality of changes in the northern hemisphere). Assuming that EKE scales with the temperature gradient at 500 hPa does give good agreement (Fig. S4), but this agreement may be coincidental because there is no obvious basis for picking

this particular level of the atmosphere, and temperature gradients at other levels of the troposphere behave quite differently. Several previous studies have linked the storm-track behavior to the distribution of the maximum Eady growth rate (2–4, 12, 24). The dry MAPE roughly scales like the integral of the maximum Eady growth rate squared (8), so that MAPE provides a means to combine baroclinicity at different levels and latitudes and to include the effects of latent heat release. Assuming that EKE scales like the maximum Eady growth rate evaluated at a specific pressure level (e.g., 850 or 500 hPa) does not give good agreement (Fig. S5).

Differences Between Climate Models. The MAPE scaling also provides insight into the intermodel scatter in changes in storm-track intensity. Such intermodel scatter has likely contributed to the somewhat divergent conclusions of past studies, in tandem with the use of different measures which focus on different physical aspects of the storm tracks (25). The varying magnitudes of changes in EKE in different models are captured by the scaling with nonconvective MAPE in JJA (Fig. 1C) and to a lesser extent for annual-mean statistics (Fig. S1C). Thus, although the exact magnitude of changes in EKE for a given increase in greenhouse gases remains unclear, it can be largely understood in terms of changes in the zonal- and time-mean temperature and moisture distributions. The fractional changes in EKE and MAPE in DJF are, however, only weakly correlated across the different models and hemispheres (Fig. S2C)[†]. The sum of squared fractional changes in nonconvective MAPE is smaller by a factor of 12 in DJF than JJA, whereas the sum of squared errors from the theoretical scaling is similar in both seasons. The similar magnitude of deviations from the scaling suggests that, although MAPE changes dominate the EKE response in JJA, other dynamical factors become relatively more important in DJF because of the small magnitude of MAPE changes in this season.

The weakening of the summer storm track in the northern hemisphere is greater in the two simulations with the Model for Interdisciplinary Research on Climate (MIROC) than for the other simulations analyzed (Fig. 1C). Indeed, the MIROC simulations show a large warming in the middle and upper troposphere in summer in the northern high latitudes (Fig. S6), which tends to decrease MAPE through changes in meridional temperature gradients and static stability. Interestingly, the MIROC simulations are also among the fastest to lose Arctic sea ice as global warming progresses (26), and the detailed nature of the relationship between the loss of Arctic sea ice and the weakening of the summer storm track requires further study; such a weakening could have regional air quality implications (11).

Discussion
I have shown how the varied changes in the intensity of extratropical storm tracks under global warming can be quantitatively related to changes in the mean state of the atmosphere. The MAPE scaling accounts for the major features of the response, including the increase in intensity of the southern storm track, the amplification of the seasonal cycle of intensity in both hemispheres, and much of the variation in response in simulations with different climate models. The introduction of the nonconvective MAPE helps to clarify whether changes in available energy are related to local overturning (convective) circulations rather than larger-scale circulations. Despite expectations that increased latent heating should "fuel" increases in extratropical storm activity under global warming, I find that the fractional changes in nonconvective MAPE are similar to those in dry MAPE, although it remains possible that increases in latent heating

Fig. 3. Changes in temperature (in kelvin) in climate model simulations of global warming in DJF and JJA. The changes shown are of zonal- and time-mean temperatures at different pressure levels and latitudes and in the multimodel mean. Decreasing temperatures in the stratosphere are not shown for clarity (the primary contribution to MAPE comes from the less statically stable troposphere).

[†]The correlation coefficient between fractional changes in EKE and nonconvective MAPE across the different models and hemispheres is 0.22 with a p value of 0.16 in DJF compared with 0.85 and 3.4×10^{-7} in JJA. The p values are based on a one-tailed test and the assumption of independent models and hemispheres.

O'Gorman

contribute more to smaller-scale storms or on a regional basis. Indeed, the increased difference between MAPE and nonconvective MAPE in the warmer climate implies greater available energy for smaller-scale convective storms, particularly in summer in the northern hemisphere. The detailed regional changes in the storm tracks have not been considered here, and would likely be difficult to account for in any simple way because of the complex dynamical processes involved (27).

The MAPE scaling should also be useful to reason about changes in storm-track intensity in past climates. Such changes could have important implications for the climate system as a whole. For example, the strength and position of the southern storm track has been posited to have a key influence on the ocean circulation and carbon cycle (9). (The mean surface wind stress is affected by the storm tracks both because it is sensitive to surface wind variance and because the mean surface winds are driven by upper-level eddy momentum fluxes.) The MAPE scaling implies that changes in storm-track intensity are sensitive to competing effects of changes in temperature gradients and static stability at different levels, so that the transient storm-track response may be quite different from the response after the surface-air temperatures have equilibrated to the change in forcing (of order 1,000 y in the southern hemisphere; ref. 28). Thus, for example, one should not use the strengthening of the southern storm track in transient global-warming simulations to infer a stronger southern storm track in an Eocene hothouse climate, or to infer a weaker southern storm track in glacial climates. A thermodynamic-based understanding of extratropical storm-track intensity in past climates may be possible, but the long-term changes in the thermal structure of the lower and upper troposphere must be taken into account.

Methods

Data and Analysis. The 11 climate models used are bccr-bcm2.0, cnrm-cm3, csiro-mk3.5, echam5/mpi-om, fgoals-g1.0, gfdl-cm2.0, gfdl-cm2.1, inm-cm3.0, miroc3.2-medres, miroc3.2-hires, and mri-cgcm2.32. Results are based on differences between the final two decades of the 20th and 21st centuries under the SRES-A1B emissions scenario (compared with 20C3M), corresponding to a global-mean surface-air temperature increase of 2.8 K in the multimodel mean. The time periods for averaging were 1981–2000 and 2081–2100 with the exceptions of bccr-bcm2.0 (1981–1998 and 2081–2098) and cnrm-cm3, miroc3.2-hires, and fgoals-g1.0 (1981–1999 and 2081–2099). The NCEP-DOE reanalysis data are based on the 2.5° spatial-resolution product from 1981–2000. Daily mean winds, monthly mean temperatures, and monthly mean relative humidities were used in all cases.

Transient EKE was calculated by high-pass filtering the daily horizontal winds using a Butterworth filter with a 6-d cutoff. Although the scaling behavior of EKE is generally insensitive to the exact choice of filter, replacing the time-filtered winds with deviations from the time mean would give qualitatively different results. Results for the vertical mass-weighted integral of EKE are reported. MAPE was calculated based on the zonal- and time-mean temperature and relative humidity (see below). Not including zonal asymmetries in the available potential energy calculation is necessary for computational efficiency, but also simplifies interpretation of the results.

EKE and MAPE were calculated over each hemisphere, but excluding the region within 20° of the equator. The subtropical cutoff latitude of 20° was chosen to allow for the seasonal migration of eddies while still excluding tropical regions with low supercriticality to baroclinic instability. Using hemispheric values (Fig. S7) or a cutoff latitude of 30° (Fig. S8) affects the scaling of MAPE and nonconvective MAPE more than dry MAPE. This dependence is unsurprising given that the cutoff latitude affects how much of the moist and potentially unstable tropics are included in the calculation. The stratosphere is not explicitly excluded for either EKE or MAPE, but the daily winds are reported only up to 200 hPa for most models.

Calculation of MAPE. The zonal- and time-mean temperature and relative humidities are first interpolated to an equal-area grid in latitude (40 latitudes) and an evenly spaced but staggered grid in pressure (40 levels) (16). The moist thermodynamic formulation includes latent heat of fusion by following the approach of Wang and Randall (29), which is to use thermodynamic formulae that imply consistent latent heats, heat capacities, and saturation vapor pressures. The MAPE calculation involves an adiabatic parcel-moving algorithm that finds a reference (minimum-enthalpy) state by starting from the top of the reference atmosphere and progressively filling it with the air parcels with the highest remaining dry or moist entropy (16). This parcel-moving algorithm does not always find the correct reference state for a moist atmosphere and a modified algorithm has been suggested (30). In fact, neither algorithm is completely general, and the original algorithm finds a reference state with lower enthalpy for the states analyzed here. Devising an efficient algorithm that can be rigorously proven to find the lowest enthalpy state in all possible cases remains as a challenge for future work. The parcel-moving algorithm is altered for the nonconvective MAPE by only choosing from air parcels that are the highest remaining air parcel in their column, and for the dry MAPE by excluding all effects of water (see Fig. S3). Note that the smaller value of nonconvective MAPE compared with full MAPE (Tables S1 and S2) does not imply that there is available energy in a column of the atmosphere at a given latitude considered in isolation (so-called generalized convective available potential energy; ref. 30). Rather, horizontal eddy motions are required for moist convection to become energetically favorable.

1. Held IM (1993) Large-scale dynamics and global warming. *Bull Am Meteorol Soc* 74:228–241.
2. Hall NMJ, Hoskins BJ, Valdes PJ, Senior CA (1994) Storm tracks in a high-resolution GCM with doubled carbon dioxide. *Q J Roy Meteor Soc* 120:1209–1230.
3. Geng Q, Sugi M (2003) Possible change of extratropical cyclone activity due to enhanced greenhouse gases and sulfate aerosols—study with a high-resolution AGCM. *J Climate* 16:2262–2274.
4. Caballero R, Langen PL (2005) The dynamic range of poleward energy transport in an atmospheric general circulation model. *Geophys Res Lett* 32:L02705.
5. Bengtsson L, Hodges KI, Roeckner E (2006) Storm tracks and climate change. *J Climate* 19:3518–3543.
6. Lambert SJ, Fyfe JC (2006) Changes in winter cyclone frequencies and strengths simulated in enhanced greenhouse warming experiments: Results from the models participating in the IPCC diagnostic exercise. *Clim Dynam* 26:713–728.
7. Li C, Battisti DS (2008) Reduced Atlantic storminess during Last Glacial Maximum: Evidence from a coupled climate model. *J Climate* 21:3561–3579.
8. O'Gorman PA, Schneider T (2008) Energy of midlatitude transient eddies in idealized simulations of changed climates. *J Climate* 21:5797–5806.
9. Russell JL, Dixon KW, Gnanadesikan A, Stouffer RJ, Toggweiler JR (2006) The southern hemisphere westerlies in a warming world: Propping open the door to the deep ocean. *J Climate* 19:6382–6390.
10. Dorland C, Tol RSJ, Palutikof JP (1999) Vulnerability of the Netherlands and Northwest Europe to storm damage under climate change. *Climatic Change* 43:513–535.
11. Leibensperger EM, Mickley LJ, Jacob DJ (2008) Sensitivity of US air quality to midlatitude cyclone frequency and implications of 1980–2006 climate change. *Atmos Chem Phys* 8:7075–7086.
12. Yin JH (2005) A consistent poleward shift of the storm tracks in simulations of 21st century climate. *Geophys Res Lett* 32:L18701.
13. McCabe GJ, Clark MP, Serreze MC (2001) Trends in northern hemisphere surface cyclone frequency and intensity. *J Climate* 14:2763–2768.
14. Wang XL, Swail VR, Zwiers FW (2006) Climatology and changes of extratropical cyclone activity: Comparison of ERA-40 with NCEP-NCAR reanalysis for 1958–2001. *J Climate* 19:3145–3166.
15. Lorenz EN (1978) Available energy and the maintenance of a moist circulation. *Tellus* 30:15–31.
16. Lorenz EN (1979) Numerical evaluation of moist available energy. *Tellus* 31:230–235.
17. Schneider T, Walker CC (2006) Self-organization of atmospheric macroturbulence into critical states of weak nonlinear eddy-eddy interactions. *J Atmos Sci* 63:1569–1586.
18. Schneider T, Walker CC (2008) Scaling laws and regime transitions of macroturbulence in dry atmospheres. *J Atmos Sci* 65:2153–2173.
19. Held IM, Soden BJ (2006) Robust responses of the hydrological cycle to global warming. *J Climate* 19:5686–5699.
20. Kanamitsu M, et al. (2002) NCEP-DOE AMIP-II reanalysis (R-2). *Bull Am Meteorol Soc* 83:1631–1643.
21. Pauluis O, Held IM (2002) Entropy budget of an atmosphere in radiative-convective equilibrium. Part I: Maximum work and frictional dissipation. *J Atmos Sci* 59:125–139.
22. Schneider T, O'Gorman PA, Levine X (2010) Water vapor and the dynamics of climate changes. *Rev Geophys* 48:RG3001.
23. Hall A (2004) The role of surface albedo feedback in climate. *J Climate* 17:1550–1568.
24. Hoskins B, Valdes P (1990) On the existence of storm-tracks. *J Atmos Sci* 47:1854–1864.
25. Ulbrich U, et al. (2008) Changing northern hemisphere storm tracks in an ensemble of IPCC climate change simulations. *J Climate* 21:1669–1679.

26. Zhang X, Walsh JE (2006) Toward a seasonally ice-covered Arctic Ocean: Scenarios from the IPCC AR4 model simulations. *J Climate* 19:1730–1747.
27. Chang EKM, Lee S, Swanson KL (2002) Storm track dynamics. *J Climate* 15:2163–2183.
28. Stouffer RJ (2004) Time scales of climate response. *J Climate* 17:209–217.
29. Wang J, Randall DA (1994) The moist available energy of a conditionally unstable atmosphere. Part II: Further analysis of GATE data. *J Atmos Sci* 51:703–710.
30. Randall DA, Wang J (1992) The moist available energy of a conditionally unstable atmosphere. *J Atmos Sci* 49:240–255.